

Self-Trapping of Charge Carriers in Semiconducting Carbon Nanotubes: Structural Analysis

Lyudmyla Adamska,^{*,†} George V. Nazin,[‡] Stephen K. Doorn,[§] and Sergei Tretiak^{†,§}

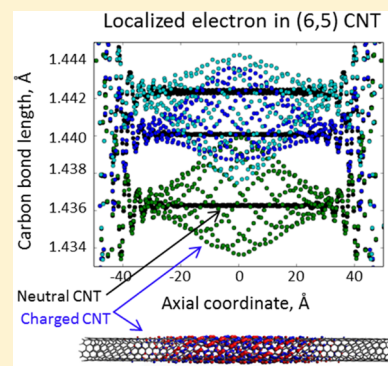
[†]Theoretical Division and Center for Nonlinear Studies, Los Alamos National Laboratory, Los Alamos, New Mexico 87545, United States

[‡]Department of Chemistry and Biochemistry, University of Oregon, 1253 University of Oregon, Eugene, Oregon 97403, United States

[§]Center for Integrated Nanotechnologies (CINT), Los Alamos National Laboratory, Los Alamos, New Mexico 87545, United States

Supporting Information

ABSTRACT: The spatial extent of charged electronic states in semiconducting carbon nanotubes with indices (6,5) and (7,6) was evaluated using density functional theory. It was observed that electrons and holes self-trap along the nanotube axis on length scales of about 4 and 8 nm, respectively, which localize cations and anions on comparable length scales. Self-trapping is accompanied by local structural distortions showing periodic bond-length alternation. The average lengthening (shortening) of the bonds for anions (cations) is expected to shift the G-mode frequency to lower (higher) values. The smaller-diameter nanotube has reduced structural relaxation due to higher carbon-carbon bond strain. The reorganization energy due to charge-induced deformations in both nanotubes is found to be in the 30–60 meV range. Our results represent the first theoretical simulation of self-trapping of charge carriers in semiconducting nanotubes, and agree with available experimental data.



Over the past few decades, many types of carbon nanotube (CNT) based devices have been engineered, among which are CNT field-effect transistors^{1–3} (FET) with performance superior to the best silicon FETs,² all-nanotube computer,⁴ CNT-based photovoltaic devices with up to 3% efficiency,^{5,6} with potential efficiencies of 17%,⁷ when CNTs, playing the role of light absorbers, are interfaced with metal oxides, just to name a few applications. Electronic properties of CNTs have been thoroughly investigated in both experimental^{8–11} and theoretical studies.^{12–14} In theoretical studies, density functional theory (DFT) and tight binding (TB) calculations frequently rely on the geometry of the system's ground state to compute the properties of excited states. A good agreement between theory^{12,15,16} and experiment¹⁷ (for example, for electron-hole correlation length, or the exciton size of about 2–4 nm) is often achieved by appropriately accounting for electronic correlations and Coulomb screening. Inclusion of vibrational-relaxation effects allows quantification of electron-phonon coupling constants^{18–20} and extraction of another length scale, namely, the localization length of the excitonic wave function at about 6–10 nm,^{21,22} or the spatial extent of excitation-induced deformation in the underlying ground state structure of the nanotube. Nanotubes are indeed rigid structures, and they do not exhibit drastic structural changes due to photoexcitation (as is the case in aromatic polymers^{23–26}). Less attention has been paid to similar lattice-deformation effects responsible for localization of charges in carbon nanotubes. Recent experimental work (using scanning tunneling spectroscopy (STS)) investigated the effect of

vibrational excitation in charge transport through quantum-confined electronic states in individual nanotubes suspended across step edges on the Au(111) substrate.²⁷ The authors were able to create real-space maps of the wave functions of electrons and holes localized in CNTs on a few-nanometer length scale, and unambiguously showed that these localized states were coupled to the vibrational degrees of freedom. Their work has motivated us to study the charged excitations in carbon nanotubes computationally in order to better understand the electronic properties of charged nanotubes.

Here, we present results of calculations for charge-carrier self-trapping (or polaron formation) in two semiconducting CNTs, (6,5) and (7,6). Our calculations show that electrons and holes localize on sub-10 nm lengths, with structural relaxation being more pronounced in the larger-diameter tube. We analyze the Peierls-like distortion of carbon-carbon bond lengths in charge localization regions and connect these deformations to distortion along a specific phonon mode. Finally, we estimate the vibrational relaxation energy of electrons and holes in small-diameter nanotubes.

Nanotubes. (6,5) and (7,6) nanotubes have chiral angles of about 27°, and diameters of 0.76 and 0.90 nm, respectively (Table 1). These CNTs are approximately armchair, with very large unit cells of about 4 nm in the axial direction. All bonds in

Received: August 7, 2015

Accepted: September 11, 2015

Table 1. Structural Properties of Considered CNTs^a

CNT	d , nm	α , degrees	bond lengths, Å			energy values, eV							
			L_{90}	L_{-30}	L_{30}	RE(+)	RE(-)	IP	EA	QEG	HL	Δ	E_{11}
(6,5)	0.757	27.00	1.4363	1.4405	1.4425	0.033	0.058	3.59	0.42	3.16	2.96	1.73	1.25
(7,6)	0.895	27.46	1.4362	1.4388	1.4407	0.037	0.054	3.43	0.64	2.79	2.60	1.48	1.11

^aDiameter of the nanotubes (d), chiral angle (α), and lengths of three groups of inequivalent bonds, which are schematically shown in Figure 1. Reorganization energies RE(+) and RE(-) are also shown for cations and anions, respectively. Ionization potential (IP), electron affinity (EA), quasiparticle energy gap (QEG), HOMO–LUMO gap (HL) were computed using CAM-B3LYP functional. Experimental fundamental band gap Δ is calculated using eq 4 fit in ref 48 and experimental optical gap E_{11} is taken from ref 49.

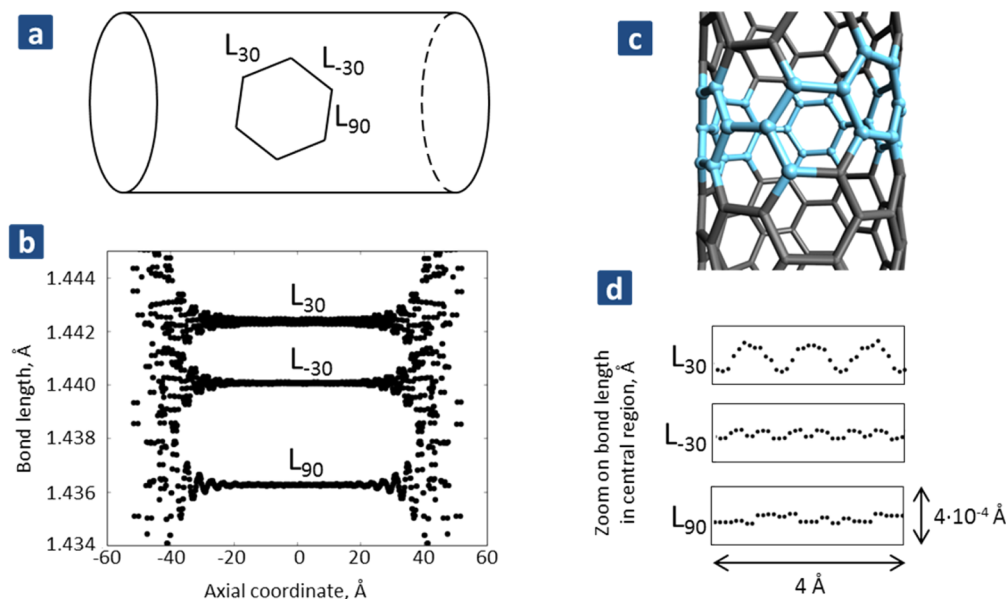


Figure 1. (a) Schematic representation of three nonequivalent groups of bonds: L_{90} , L_{-30} , and L_{30} . The subscript denotes the approximate angle between the bond and nanotube axis. (b) Bond lengths of these three groups of bonds as a function of tube's axial coordinate in (6,5) CNT. (c) The unit of approximate periodicity of bond length alternation is highlighted in blue. This area contains 33 carbon atoms, 16 L_{90} bonds, and 11 of each of $L_{\pm 30}$ bonds. (d) Zoom on three groups of bonds in 4 Å long center region.

these CNTs can be classified into three main groups: L_{90} , L_{-30} , and L_{30} , with the subscript corresponding to the approximate angle between the bond and the axis of the nanotube, as schematically shown in Figure 1a. The L_{90} bonds have the shortest bond length, L_{-30} bonds are longer, and L_{30} are the longest bonds, as can be seen from Figure 1b and Table 1, where we plot the nearest-neighbor distance in (6,5) nanotube as a function of the axial coordinate. Bond lengths in the central region of the neutral nanotube, a close-up of which is shown in Figure 1d, show a distortion similar to that observed for metallic^{28,29} and semiconducting²² nanotubes, but with smaller magnitude ($\sim 10^{-4}$ Å). Indeed, in previous calculations on finite-length nanotubes,^{28,30–32} very short tube segments were used, and periodic bond length alternation with higher magnitude of about 2×10^{-2} Å were observed.^{28,30} The smaller magnitude of bond distortion obtained in our calculations on longer nanotubes therefore suggests that large distortions in short nanotube segments observed previously may have been caused by edge relaxation, which is seen in Figure 1b as large oscillations in the bond lengths near the free edges of the nanotube. This perturbation spreads toward the center of the CNTs by about 3 nm, which leaves a center region of 4 nm unaffected by edge effects in the simulated CNTs. This center region of neutral CNTs shows periodic variations in the bond length, on a scale of $\sim 10^{-4}$ Å (Figure 1d). In a neutral (6,5) CNT, the periodicity of these variations

for L_{90} bonds is 16 bonds, and for $L_{\pm 30}$ bonds the periodicity is 11 bonds. This approximately corresponds to one rotation around the CNT circumference, as schematically shown in Figure 1c.

Structural Distortion in CNT Due to Positive and Negative Charges. In the presence of a localized charge, the equilibrated bond lengths were found to be strongly distorted, as shown in Figure 2. In positively charged nanotubes (Figures 2a,e and S3) the carbon–carbon bond lengths of all three families of bonds deviate from their measurements in the neutral tubes by up to 0.002 Å, the effect being most pronounced in the center of the tube. The natural orbital, e.g., the wave function of an unpaired electron (Figure 2b,f), is spread almost over the entire tube, which correlates with the bond deformation pattern (Figure 2a,e). From these figures, we extract that the localization length of the positive charge in the nanotube is about 8 nm. In negatively charged nanotubes (Figures 2c,g and S3), all three families of bonds are highly distorted in the central region. The natural orbitals are localized on the nanotube center fragments that experience large distortions in the carbon–carbon bond lengths. The localization length of the negative charge is about 4 nm in both (7,6) and (6,5) nanotubes. We note that the (6,5) CNT has slightly longer geometry-distortion lengths for both charge polarities due to higher strain in carbon–carbon bonds increasing the rigidity of the nanotube structure. Here 4 and 8 nm are defined as maximal lengths of tube segment affects by

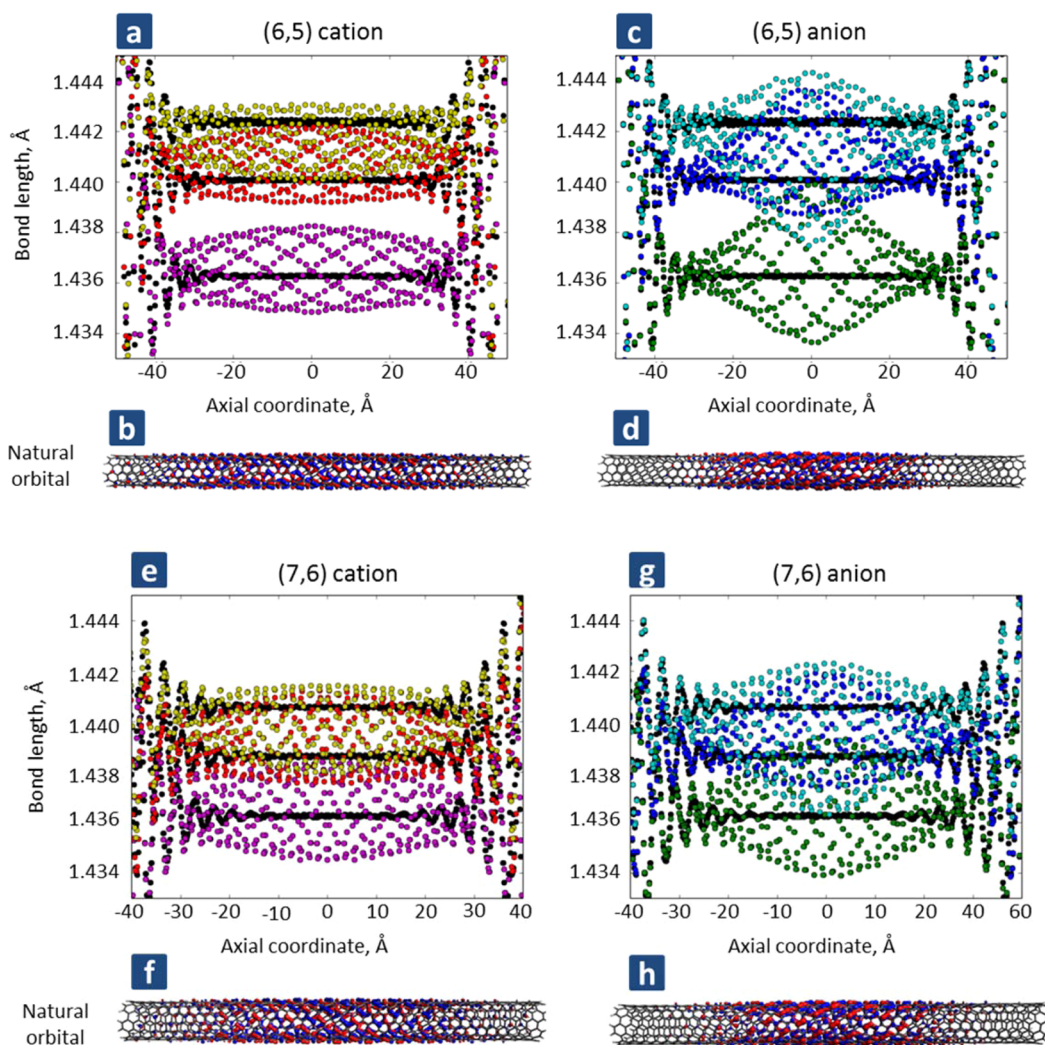


Figure 2. Bond lengths in positively and negatively charged (6,5) and (7,6) nanotubes as a function of tube's axial coordinate. Bond lengths in the neutral nanotubes are shown in black circles for comparison. Wave function of the unpaired electron in positively and negatively charged nanotubes are shown under each bond length plot.

geometry relaxation and concomitant spreads of the respective natural orbitals (Figure 2). Alternative definitions such as full width at half maximum (fwhm) will provide smaller values.

The obtained bond-length distortion patterns are strikingly different from those reported in previous simulations of the geometries of charged CNTs. In particular, simulation of a 2 nm (5,5) metallic nanotube reported significant L_{90} bond alternations in neutral CNT states, with different possible isomers showing distinctly different patterns.²⁸ Reduction of the Peierls distortion for L_{90} bonds due to the negative charge was also observed.²⁸ In contrast, our results do not show significant bond alternations in neutral CNTs, but instead show bond alternations similar to those of ref 28 in the charged states of studied CNTs (Figure S2).

In addition to the bond-length alternations, charged CNTs experience a twisting deformation (Figure 3). Comparison of Figures 2 and 3 shows that in charged CNTs, carbon atoms located in the areas of charge localization “twist” out of their neutral positions, whereas the terminal regions do not show bond-length alternation or twist-like deformation of bonds.

It is important to note that the charges do localize in nanotubes that are geometry-optimized using the CAM-B3LYP functional, and do not localize when calculations are done with

the B3LYP functional, which demonstrates the inability of the B3LYP functional to address molecular properties beyond the ground state, as can be seen from Figure 3. These observations are concomitant to previous DFT studies of electronic excitations of conjugated polymers.^{23–26} The absence of saturation in the twist angle in B3LYP-relaxed systems in Figure 3 correlates with bond-length alternation taking place along the entire 10 nm CNT length (Figure S4 and S5).

Electronic Properties of Charged CNTs. We have calculated the ionization potential (IP) and electron affinity (EA) for the nanotubes with localized charges. The IP and EA were computed as differences in total energies E_{tot} between the neutral nanotube (G^0) and geometry-optimized charged nanotube (G^\pm): $\text{IP} = E_{\text{tot}}(G^+) - E_{\text{tot}}(G^0)$, $\text{EA} = E_{\text{tot}}(G^0) - E_{\text{tot}}(G^-)$. The computed values of IP are 3.6 and 3.4 eV for (6,5) and (7,6) nanotubes, respectively. The calculated EA values are 0.4 and 0.6 eV in (6,5) and (7,6) CNTs, respectively. This allows us to calculate the CNT quasiparticle energy gap ($\text{QEG} = \text{IP} - \text{EA}$), which can be compared to the experimental band gap Δ (see Table 1). As expected, our calculations overestimate the fundamental gap by more than 1 eV (which is common for range-corrected functionals); however, the trend is correct: the thinner nanotube has a larger bandgap.

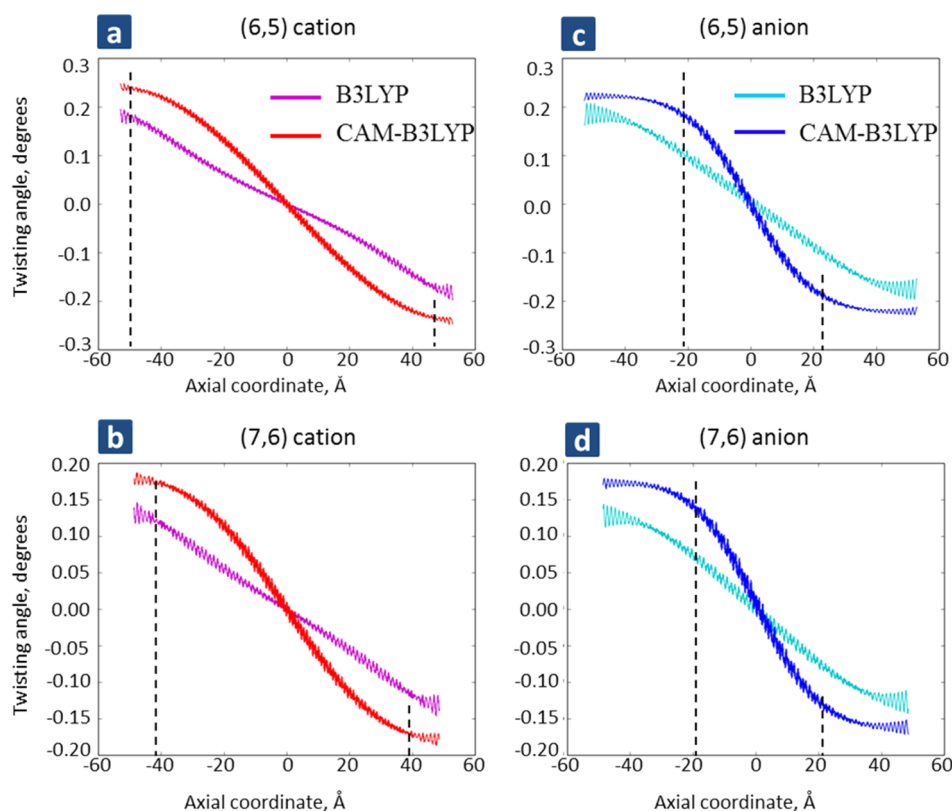


Figure 3. Twist angle, or change in chiral angle, (degrees) in charged tubes compared to neutral tubes. The coordinates of carbon atoms (x, y, z) were converted to cylindrical coordinate systems (r, ϕ, h). The position of carbon atom along CNT axis is contained in axial coordinate h , and the polar angle is denoted as ϕ . Panels a–d thus show the difference in polar angle along tube axis between neutral and charged CNTs. The chirality of the tube and sign of charge is labeled above each subplot.

Since charge carriers in the studied CNTs localize on a few-nanometer length scale, one can expect that for nanotube segments shorter than that, the electronic properties should depend on their lengths. Indeed, DFT calculations yield the IPs of finite-length nanotubes to be size-dependent,^{28,30–32} shifting to larger values in shorter tubes in accordance with the effect of IP scaling as a function of the system size that is known for organic molecules.

We have also calculated the reorganization energy (RE)—the vibrational relaxation energy associated with charge-induced deformations (Table 1). The reorganization energy for cation RE(+) reflects the changes in total energies of charged CNTs G^+ in neutral geometry G^0 , denoted as $(G^+[G^0])$, and neutral nanotubes in relaxed charged geometry $(G^0[G^+])$, and is expressed using the following formula: $RE(+) = E_{\text{tot}}(G^0[G^+]) - E_{\text{tot}}(G^0) + E_{\text{tot}}(G^+[G^0]) - E_{\text{tot}}(G^+)$. RE(–) is defined in an analogous way: $RE(-) = E_{\text{tot}}(G^0) - E_{\text{tot}}(G^0[G^-]) + E_{\text{tot}}(G^-[G^0]) - E_{\text{tot}}(G^-)$. By construction, RE(\pm) thus quantifies the vibrational relaxation energy of the CNT due to charge-induced deformations and does not include the environmental effects. Our RE definition is consistent with Marcus theory. The total vibrational relaxation energy due to one localized charge would be half of our RE in the case of harmonic approximation. We find that the electron and hole states reorganization energies are 55 and 35 meV, respectively, upon CNT charging. Naturally, an electron creates larger lattice distortion compared to a hole. The contributions from $E_{\text{tot}}(G^0[G^\pm]) - E_{\text{tot}}(G^0)$ and $E_{\text{tot}}(G^\pm[G^0]) - E_{\text{tot}}(G^\pm)$ differ by 1 meV, thus the harmonic approximation holds.

Phonon Modes Associated with Charge-Induced Lattice Deformations. The calculations of phonon modes in 10 nm long CNTs is an intractable task at the current state of computational technology, therefore here we attempt to establish a qualitative relation between the active phonon modes and geometrical distortions in CNTs caused by charge-induced bond-length alternations. The results of our calculations allow us to identify the major phonon mode associated with charged geometries as a Kekule-band mode (often referred to as the D-band phonon). Indeed, in previous theoretical work,^{28,30–32} where short armchair nanotubes were used, Kekule order was responsible for a short–short–long and long–long–short rippling deformation. In the present work, we find that in the case of a positive charge, a hole is extracted from bonds of Kekule rings, and therefore those bonds become longer than non-Kekule bonds (even though the average bond length is decreased), as shown in Figure 4a. In the case of negative charge, an “extra” negative charge is added to the bonds of Kekule rings, which reduces the lengths of these bonds as compared to other bonds (Figure 4b). Support for this picture is provided by experiments on STS spectroscopy of charge transport through individual carbon nanotubes, where vibrational overtones consistent with Kekule-band phonons were observed.²⁷ Indeed, the appearance of particular vibrations in STS spectra is associated with the local structural deformation occurring upon the transient charging of the nanotube, with the magnitudes of the vibrational overtones determined by the appropriate Franck–Condon factors.³³

Our results are also directly relevant to studies of Raman scattering in charged³⁴ and electrochemically doped³⁵ carbon

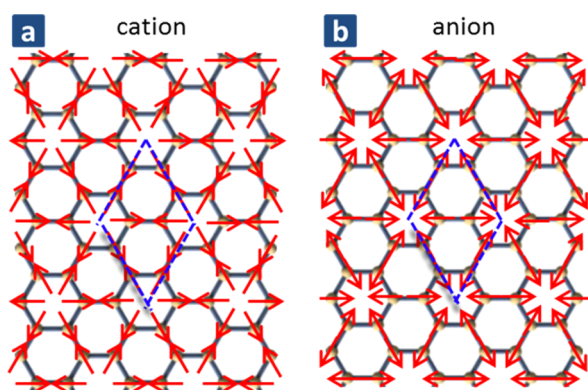


Figure 4. Schematic representation of phonon modes in cation (a) and anion (b), which would lead to observed bond alternation patterns.

nanotube bundles, where it was shown that the G-band phonon mode shifts to higher frequency in positively charged nanotubes, and to lower frequency in negatively charged nanotubes. These observations were attributed to bond lengthening and contraction in negatively and positively doped CNTs, respectively,^{34,35} which is corroborated by our results. Indeed, our calculations show that the bond lengths in the positively charged CNT are, on average, shorter (Figure S6a), which should result in increased elastic constants for carbon–carbon bonds, and thus increased G-band phonon frequency. In the negatively charged CNT, the average bond lengths are slightly longer (Figure S6b), which should result in a decrease of the G-band phonon frequency.

Another experimental observation of ref 34 is a wide unidentified phonon band with frequencies 900–1300 cm^{-1} present in negatively charged CNT bundles, and absent in uncharged bundles. This band was identified as intermediate frequency modes (IFM) in later studies. We suggest that this band may be related to softened (due to the presence of negative charge) and broadened D-band phonon modes,²⁷ as well as intermediate frequency modes,^{35,36} that are activated by lattice deformations caused by the localized electrons. The large width of this band could be a result of combined contributions from individual tubes in the bundle.

Discussion. The main observations of this work are (i) inequivalence of electron and hole coupling to structural degrees of freedom in small diameter carbon nanotubes and (ii) tube diameter-dependent trends of electron and hole localization lengths and reorganization energies. In particular, RE of holes increases from 33 meV in (6,5) CNT ($d = 0.76$ nm) to 37 meV in (7,6) ($d = 0.9$ nm). The opposite trend takes place in RE of electrons: 58 meV in (6,5) and 54 meV in (7,6). As the tube diameter increased from 0.76 to 0.9 nm, RE(+) increased by 4 meV, and RE(–) decreased by the same amount. The qualitative extrapolation to larger diameter nanotubes yields RE(+) \approx RE(–) \approx 46 meV in CNTs with diameter 1.2 nm or larger.

Our results for relaxation energies are similar to those obtained by Perebeinos, Tersoff, and Avouris,³⁷ who used tight-binding calculation to evaluate the polaronic band gap renormalization caused by electron–phonon (e – ph) interaction. Following ref 38, the authors set the e – ph coupling proportional to $N^{-1/2}$, where N was the number of primitive unit cells, thus the e – ph interaction is inversely proportional to the square root of the tube diameter. The authors show that the

largest correction to the electronic energy (up to ~ 70 meV for higher-energy electrons) comes from electron coupling to K-point longitudinal optical phonons corresponding to the Kekule-band phonons described above, consistent with our results. Energy correction for low-energy charge carriers calculated in ref 38 gives band gap renormalization of ~ 35 meV, comparable to the total vibrational relaxation energies calculated in our work. However, in contrast to our results, the band gap renormalization obtained in ref 38 is dominated by coupling to acoustic and breathing-mode phonons near the Γ point, which is not expected to produce bond-alternations such as those shown in Figure 2 and 4. We attribute this qualitative discrepancy to the perturbative nature of calculations reported in ref 38, which do not take into account the apparent breaking of CNT symmetry observed in our work. Indeed, dimerization shown in Figure 4 can be expected to lead to electronic intervalley coupling and Jahn–Teller symmetry-breaking involving the (D-band) phonon modes.

Finally, we emphasize that our simulations were performed in the gas phase to relate to the recent experimental STS work on charge transport in suspended nanotubes.²⁷ Polarization effects in the condensed phase should reduce the charge localization length even further. For example, calculations performed for conjugated polymers using the CAM-B3LYP model demonstrated reduction of polaron localization length from 3 to 2 repeat units in poly(phenylene vinylene)s.²⁷ The recent experimental study of Deria et al.³⁹ reported measurements of the optoelectronic properties of hole-doped chirality-enriched nanotubes. Following the theoretical model in ref 40, which relates the band gap renormalization to the amount of hole density per unit length, the authors deduced the maximal doping of holes in CNTs to be ~ 0.36 holes/nm, or 1 hole per about 3 nm. These results suggest enhancement of charge localization due to dielectric screening from surfactants and solvent environment as well as direct Coulomb interactions between charge carriers.

In summary, we have studied, for the first time, the self-trapping of positive and negative charges in long semi-conducting carbon nanotubes leading to the formation of polaronic states. We find that electrons and holes localize on ~ 4 nm and ~ 8 nm length scales in vacuum, respectively. Electrons are not only more localized, but also create larger distortions in carbon–carbon bond lengths, and have larger vibrational relaxation energy due to structural distortions caused by added charges. Observed localization lengths are expected to be even smaller in the presence of dielectric environment such as surfactants, solvent or DNA/polymer functionalization. Localized cations and anions result in formation of bond-length alternation patterns, which can be considered as a deformation along the vibrational coordinate corresponding to the D-band (Kekule) phonon mode. Smaller-diameter nanotubes have smaller geometry relaxation because charge-induced distortions compete with larger strain in carbon–carbon bonds. We have shown that in order to accurately reproduce the local structural relaxation, finite CNT lengths significantly longer than those often used in the literature are necessary. We believe that our results will contribute toward the more complete understanding of CNT charge carrier transport and localization, especially at the sub-10 nm length scale.

METHODS

The electronic structure calculations were performed using Gaussian 09 simulation suite⁴¹ with STO-3G basis set and two functionals: B3LYP⁴² and CAM-B3LYP,⁴³ the latter being long-range corrected, i.e., at short distances it behaves like B3LYP with 20% of orbital exchange, whereas at long distances it acquires 65% of orbital exchange, which is crucially important for the correct description of excitons and polarons in organic low-dimensional and low-dielectric constant materials.^{25,26,44} B3LYP functional, due to its small fraction of orbital exchange, overdelocalizes the wave functions of electronic excitations, which frequently leads to unphysical results.⁴⁵ In contrast, range-separated functionals (such as CAM-B3LYP) and range-tuned functionals^{45,46} provide a comprehensive molecular picture of excitations such as excitons and polarons.

Approximately 10 nm long (6,5) and (7,6) nanotubes were built using Avogadro software.⁴⁷ The edges were terminated by hydrogen atoms.¹⁶ The structures of both neutral and charged species were geometry-optimized using B3LYP and CAM-B3LYP models. Because of excessive high spin-contamination, restricted open-shell methodology was used for CAM-B3LYP calculations. Unless explicitly mentioned otherwise, all results presented refer to calculations with restricted open-shell CAM-B3LYP.

ASSOCIATED CONTENT

Supporting Information

The Supporting Information is available free of charge on the ACS Publications website at DOI: 10.1021/acs.jpcllett.5b01729.

Structural properties of charged carbon nanotubes; comparison of electronic properties of CNTs computed with B3LYP and CAM-B3LYP functionals; averaged bond lengths distribution (PDF)

AUTHOR INFORMATION

Notes

The authors declare no competing financial interest.

ACKNOWLEDGMENTS

L.A. acknowledges Jin Liu for his help with simulations. This work was supported by the U.S. Department of Energy and Los Alamos LDRD funds. Los Alamos National Laboratory is operated by Los Alamos National Security, LLC, for the National Nuclear Security Administration of the U.S. Department of Energy under contract DE-AC5206NA25396. We acknowledge support from the Center for Integrated Nanotechnologies (CINT) and the Center for Nonlinear Studies (CNLS) at LANL. G.V.N. acknowledges support by NSF CAREER award CHE-1454036.

REFERENCES

- (1) Postma, H. W. C.; Teepen, T.; Yao, Z.; Grifoni, M.; Dekker, C. Carbon Nanotube Single-Electron Transistors at Room Temperature. *Science* **2001**, *293* (5527), 76–79.
- (2) Franklin, A. D.; Luisier, M.; Han, S.-J.; Tulevski, G.; Breslin, C. M.; Gignac, L.; Lundstrom, M. S.; Haensch, W. Sub-10 nm Carbon Nanotube Transistor. *Nano Lett.* **2012**, *12* (2), 758–762.
- (3) Franklin, A. D.; Farmer, D. B.; Haensch, W. Defining and Overcoming the Contact Resistance Challenge in Scaled Carbon Nanotube Transistors. *ACS Nano* **2014**, *8* (7), 7333–7339.
- (4) Shulaker, M. M.; Hills, G.; Patil, N.; Wei, H.; Chen, H.-Y.; Wong, H. S. P.; Mitra, S. Carbon nanotube computer. *Nature* **2013**, *501* (7468), 526–530.
- (5) Ye, Y.; Bindl, D. J.; Jacobberger, R. M.; Wu, M.-Y.; Roy, S. S.; Arnold, M. S. Semiconducting Carbon Nanotube Aerogel Bulk Heterojunction Solar Cells. *Small* **2014**, *10* (16), 3299–3306.
- (6) Gong, M.; Shastry, T. A.; Xie, Y.; Bernardi, M.; Jason, D.; Luck, K. A.; Marks, T. J.; Grossman, J. C.; Ren, S.; Hersam, M. C. Polychiral Semiconducting Carbon Nanotube–Fullerene Solar Cells. *Nano Lett.* **2014**, *14* (9), 5308–5314.
- (7) Wang, F.; Kozawa, D.; Miyauchi, Y.; Hiraoka, K.; Mouri, S.; Ohno, Y.; Matsuda, K. Considerably improved photovoltaic performance of carbon nanotube-based solar cells using metal oxide layers. *Nat. Commun.* **2015**, *6*, 6305.
- (8) Dresselhaus, M. S.; Dresselhaus, G.; Eklund, P. C.; Rao, A. M. Carbon Nanotubes. In *The Physics of Fullerene-Based and Fullerene-Related Materials*; Andreoni, W., Ed.; Springer: Netherlands, 2000; Vol. 23, pp 331–379.
- (9) Dresselhaus, M. S.; Eklund, P. C. Phonons in carbon nanotubes. *Adv. Phys.* **2000**, *49* (6), 705–814.
- (10) Terrones, M. SCIENCE AND TECHNOLOGY OF THE TWENTY-FIRST CENTURY: Synthesis, Properties, and Applications of Carbon Nanotubes. *Annu. Rev. Mater. Res.* **2003**, *33* (1), 419–501.
- (11) De Volder, M. F. L.; Tawfik, S. H.; Baughman, R. H.; Hart, A. J. Carbon Nanotubes: Present and Future Commercial Applications. *Science* **2013**, *339* (6119), 535–539.
- (12) Perebeinos, V.; Tersoff, J.; Avouris, P. Scaling of Excitons in Carbon Nanotubes. *Phys. Rev. Lett.* **2004**, *92* (25), 257402.
- (13) Louie, S. Electronic Properties, Junctions, and Defects of Carbon Nanotubes. In *Carbon Nanotubes*, Dresselhaus, M.; Dresselhaus, G.; Avouris, P., Eds.; Springer: Berlin Heidelberg, 2001; Vol. 80, pp 113–145.
- (14) Benedict, L. X.; Louie, S. G.; Cohen, M. L. Static polarizabilities of single-wall carbon nanotubes. *Phys. Rev. B: Condens. Matter Mater. Phys.* **1995**, *52* (11), 8541–8549.
- (15) Capaz, R. B.; Spataru, C. D.; Ismail-Beigi, S.; Louie, S. G. Diameter and chirality dependence of exciton properties in carbon nanotubes. *Phys. Rev. B: Condens. Matter Mater. Phys.* **2006**, *74* (12), 121401.
- (16) Kilina, S.; Tretiak, S. Excitonic and Vibrational Properties of Single-Walled Semiconducting Carbon Nanotubes. *Adv. Funct. Mater.* **2007**, *17* (17), 3405–3420.
- (17) Luer, L.; Hoseinkhani, S.; Polli, D.; Crochet, J.; Hertel, T.; Lanzani, G. Size and mobility of excitons in (6, 5) carbon nanotubes. *Nat. Phys.* **2009**, *5* (1), 54–58.
- (18) Yin, Y.; Vamivakas, A. N.; Walsh, A. G.; Cronin, S. B.; Ünlü, M. S.; Goldberg, B. B.; Swan, A. K. Optical Determination of Electron-Phonon Coupling in Carbon Nanotubes. *Phys. Rev. Lett.* **2007**, *98* (3), 037404.
- (19) Shreve, A. P.; Haroz, E. H.; Bachilo, S. M.; Weisman, R. B.; Tretiak, S.; Kilina, S.; Doorn, S. K. Determination of Exciton-Phonon Coupling Elements in Single-Walled Carbon Nanotubes by Raman Overtone Analysis. *Phys. Rev. Lett.* **2007**, *98* (3), 037405.
- (20) Lüer, L.; Gadermaier, C.; Crochet, J.; Hertel, T.; Brida, D.; Lanzani, G. Coherent Phonon Dynamics in Semiconducting Carbon Nanotubes: A Quantitative Study of Electron-Phonon Coupling. *Phys. Rev. Lett.* **2009**, *102* (12), 127401.
- (21) Chang, E.; Bussi, G.; Ruini, A.; Molinari, E. Excitons in Carbon Nanotubes: An *Ab Initio* Symmetry-Based Approach. *Phys. Rev. Lett.* **2004**, *92* (19), 196401.
- (22) Tretiak, S.; Kilina, S.; Piryatinski, A.; Saxena, A.; Martin, R. L.; Bishop, A. R. Excitons and Peierls Distortion in Conjugated Carbon Nanotubes. *Nano Lett.* **2007**, *7* (1), 86–92.
- (23) Adamska, L.; Nayyar, I.; Chen, H.; Swan, A. K.; Oldani, N.; Fernandez-Alberti, S.; Golder, M. R.; Jasti, R.; Doorn, S. K.; Tretiak, S. Self-Trapping of Excitons, Violation of Condon Approximation, and Efficient Fluorescence in Conjugated Cycloparaphenylenes. *Nano Lett.* **2014**, *14* (11), 6539–6546.
- (24) Liu, J.; Adamska, L.; Doorn, S. K.; Tretiak, S. Singlet and triplet excitons and charge polarons in cycloparaphenylenes: a density functional theory study. *Phys. Chem. Chem. Phys.* **2015**, *17* (22), 14613–14622.

- (25) Nayyar, I. H.; Batista, E. R.; Tretiak, S.; Saxena, A.; Smith, D. L.; Martin, R. L. Role of Geometric Distortion and Polarization in Localizing Electronic Excitations in Conjugated Polymers. *J. Chem. Theory Comput.* **2013**, *9* (2), 1144–1154.
- (26) Nayyar, I. H.; Batista, E. R.; Tretiak, S.; Saxena, A.; Smith, D. L.; Martin, R. L. Localization of Electronic Excitations in Conjugated Polymers Studied by DFT. *J. Phys. Chem. Lett.* **2011**, *2* (6), 566–571.
- (27) Kisilitsyn, D. A.; Hackley, J. D.; Nazin, G. V. Vibrational Excitation in Electron Transport through Carbon Nanotube Quantum Dots. *J. Phys. Chem. Lett.* **2014**, *5* (18), 3138–3143.
- (28) Zhou, Z.; Steigerwald, M.; Hybertsen, M.; Brus, L.; Friesner, R. A. Electronic Structure of Tubular Aromatic Molecules Derived from the Metallic (5,5) Armchair Single Wall Carbon Nanotube. *J. Am. Chem. Soc.* **2004**, *126* (11), 3597–3607.
- (29) Mintmire, J. W.; Dunlap, B. I.; White, C. T. Are fullerene tubules metallic? *Phys. Rev. Lett.* **1992**, *68* (5), 631–634.
- (30) Petrushenko, I. K.; Ivanov, N. A. Ionization potentials and structural properties of finite-length single-walled carbon nanotubes: DFT study. *Phys. E* **2013**, *54* (0), 262–266.
- (31) Matsuo, Y.; Tahara, K.; Nakamura, E. Theoretical Studies on Structures and Aromaticity of Finite-Length Armchair Carbon Nanotubes. *Org. Lett.* **2003**, *5* (18), 3181–3184.
- (32) Buonocore, F.; Trani, F.; Ninno, D.; Di Matteo, A.; Cantele, G.; Iadonisi, G. Ab initio calculations of electron affinity and ionization potential of carbon nanotubes. *Nanotechnology* **2008**, *19* (2), 025711.
- (33) Qiu, X. H.; Nazin, G. V.; Ho, W. Vibronic states in single molecule electron transport. *Phys. Rev. Lett.* **2004**, *92* (20), 206102.
- (34) Rao, A. M.; Eklund, P. C.; Bandow, S.; Thess, A.; Smalley, R. E. Evidence for charge transfer in doped carbon nanotube bundles from Raman scattering. *Nature* **1997**, *388* (6639), 257–259.
- (35) Kavan, L.; Dunsch, L. Spectroelectrochemistry of Carbon Nanotubes. *ChemPhysChem* **2011**, *12* (1), 47–55.
- (36) Lim, Y.-S.; Nugraha, A. R. T.; Cho, S.-J.; Noh, M.-Y.; Yoon, E.-J.; Liu, H.; Kim, J.-H.; Telg, H.; Háróz, E. H.; Sanders, G. D.; Baik, S.-H.; Kataura, H.; Doorn, S. K.; Stanton, C. J.; Saito, R.; Kono, J.; Joo, T. Ultrafast Generation of Fundamental and Multiple-Order Phonon Excitations in Highly Enriched (6,5) Single-Wall Carbon Nanotubes. *Nano Lett.* **2014**, *14* (3), 1426–1432.
- (37) Perebeinos, V.; Tersoff, J.; Avouris, P. Electron-Phonon Interaction and Transport in Semiconducting Carbon Nanotubes. *Phys. Rev. Lett.* **2005**, *94* (8), 086802.
- (38) Mahan, G. D. Electron-optical phonon interaction in carbon nanotubes. *Phys. Rev. B: Condens. Matter Mater. Phys.* **2003**, *68* (12), 125409.
- (39) Deria, P.; Olivier, J.-H.; Park, J.; Therien, M. J. Potentiometric, Electronic, and Transient Absorptive Spectroscopic Properties of Oxidized Single-Walled Carbon Nanotubes Helically Wrapped by Ionic, Semiconducting Polymers in Aqueous and Organic Media. *J. Am. Chem. Soc.* **2014**, *136* (40), 14193–14199.
- (40) Spataru, C. D.; Léonard, F. Tunable Band Gaps and Excitons in Doped Semiconducting Carbon Nanotubes Made Possible by Acoustic Plasmons. *Phys. Rev. Lett.* **2010**, *104* (17), 177402.
- (41) Frisch, M. J.; Trucks, G. W.; Schlegel, H. B.; Scuseria, G. E.; Robb, M. A.; Cheeseman, J. R.; Scalmani, G.; Barone, V.; Mennucci, B.; Petersson, G. A.; Nakatsuji, H.; Caricato, M.; Li, X.; Hratchian, H. P.; Izmaylov, A. F.; Bloino, J.; Zheng, G.; Sonnenberg, J. L.; Hada, M.; Ehara, M.; Toyota, K.; Fukuda, R.; Hasegawa, J.; Ishida, M.; Nakajima, T.; Honda, Y.; Kitao, O.; Nakai, H.; Vreven, T.; Montgomery Jr., J. A.; Peralta, J. E.; Ogliaro, F.; Bearpark, M. J.; Heyd, J.; Brothers, E. N.; Kudin, K. N.; Staroverov, V. N.; Kobayashi, R.; Normand, J.; Raghavachari, K.; Rendell, A. P.; Burant, J. C.; Iyengar, S. S.; Tomasi, J.; Cossi, M.; Rega, N.; Millam, N. J.; Klene, M.; Knox, J. E.; Cross, J. B.; Bakken, V.; Adamo, C.; Jaramillo, J.; Gomperts, R.; Stratmann, R. E.; Yazyev, O.; Austin, A. J.; Cammi, R.; Pomelli, C.; Ochterski, J. W.; Martin, R. L.; Morokuma, K.; Zakrzewski, V. G.; Voth, G. A.; Salvador, P.; Dannenberg, J. J.; Dapprich, S.; Daniels, A. D.; Farkas, Ö.; Foresman, J. B.; Ortiz, J. V.; Cioslowski, J.; Fox, D. J. *Gaussian 09*; Gaussian, Inc.: Wallingford, CT, 2009.
- (42) Lee, C.; Yang, W.; Parr, R. G. Development of the Colle-Salvetti correlation-energy formula into a functional of the electron density. *Phys. Rev. B: Condens. Matter Mater. Phys.* **1988**, *37* (2), 785–789.
- (43) Yanai, T.; Tew, D. P.; Handy, N. C. A new hybrid exchange–correlation functional using the Coulomb-attenuating method (CAM-B3LYP). *Chem. Phys. Lett.* **2004**, *393* (1–3), 51–57.
- (44) Ramirez, J.; Mayo, M. L.; Kilina, S.; Tretiak, S. Electronic structure and optical spectra of semiconducting carbon nanotubes functionalized by diazonium salts. *Chem. Phys.* **2013**, *413* (0), 89–101.
- (45) Autschbach, J.; Srebro, M. Delocalization Error and “Functional Tuning” in Kohn–Sham Calculations of Molecular Properties. *Acc. Chem. Res.* **2014**, *47* (8), 2592–2602.
- (46) Moore, B.; Charaf-Eddin, A.; Planchat, A.; Adamo, C.; Autschbach, J.; Jacquemin, D. Electronic Band Shapes Calculated with Optimally Tuned Range-Separated Hybrid Functionals. *J. Chem. Theory Comput.* **2014**, *10* (10), 4599–4608.
- (47) Hanwell, M.; Curtis, D.; Lonie, D.; Vandermeersch, T.; Zurek, E.; Hutchison, G. Avogadro: an advanced semantic chemical editor, visualization, and analysis platform. *J. Cheminf.* **2012**, *4* (1), 17.
- (48) Dukovic, G.; Wang, F.; Song, D.; Sfeir, M. Y.; Heinz, T. F.; Brus, L. E. Structural Dependence of Excitonic Optical Transitions and Band-Gap Energies in Carbon Nanotubes. *Nano Lett.* **2005**, *5* (11), 2314–2318.
- (49) Weisman, R. B.; Bachilo, S. M. Dependence of Optical Transition Energies on Structure for Single-Walled Carbon Nanotubes in Aqueous Suspension: An Empirical Kataura Plot. *Nano Lett.* **2003**, *3* (9), 1235–1238.